Bayesian reconstruction of impact parameter distributions from two observables for intermediate energy heavy ion collisions

Xiang Chen,[1,*] Li Li,[1,*] Ying Cui,[1,†] Junping Yang,[1] Zhuxia Li,[1] and Yingxun Zhang[1,2,‡]
[1]*China Institute of Atomic Energy, P.O. Box 275(18), Beijing 102413, China*
[2]*Department of Physics and Technology, Guangxi normal University, Guilin 540101, China*

(Received 26 October 2022; revised 18 July 2023; accepted 31 July 2023; published 13 September 2023)

To reconstruct the impact parameter distributions from the selected events sample or centrality, which is defined by two observables, at intermediate energy heavy ion collisions, we extend the approach proposed by Das *et al.* [Phys. Rev. C **97**, 014905 (2018)], Rogly *et al.* [Phys. Rev. C **98**, 024902 (2018)], and Frankland *et al.* [Phys. Rev. C **104**, 034609 (2021)]. Based on deep investigations of the fluctuation mechanism, we found that the intrinsic fluctuations are mainly generated in the microscopic stochasticity of initialization and nucleon-nucleon collisions in the nonequilibrium process of heavy ion collisions, and this leads the observables to fluctuate with respect to impact parameter in a Gaussian form. In this work, the multiplicity of the charged particles and the total transverse momentum of the light charged particles are used simultaneously to model-independently reconstruct the impact parameter distributions for selected events or centrality based on the Bayesian method. For sorting the centrality with two observables, we propose to use the K-means clustering method (an unsupervised machine learning algorithm), which can automatically sort events when the class number is given. Furthermore, the reconstructed impact parameter distributions from data of the two observables can be used to learn the correlation between multiplicity and transverse momentum at different centralities, which may be useful for understanding the fragmentation mechanism.

DOI: 10.1103/PhysRevC.108.034613

I. INTRODUCTION

Intermediate energy heavy ion collisions (HICs) provide a unique way to learn the equation of state (EoS) of bulk nuclear matter in the laboratory. In more detail, the strategy for learning EoS in the laboratory is to compare the data of selected collisions with the predictions of transport models. To get a reliable constraint on the EoS, two aspects should be investigated or considered. One is to understand the uncertainties from transport models, which stimulates the transport model evaluation project (TMEP) [1–6], and some important progresses have been made in the treatment of the nucleonic mean field [4] and the collision [5,6]. The other is to simulate the HICs with the same conditions as in experiments, for example, the same impact parameter distributions. This also stimulates studies on how to sort or estimate the impact parameter distributions for reducing the uncertainties due to the mismatch of experimental centrality in transport model simulations [7–12].

The impact parameter b is not directly measurable and is usually estimated from a single observable or multiple observables with different methods. Generally, the methods for estimating impact parameters or reconstructing impact parameter distributions can be divided into three types [13]. The first one is the sharp cutoff approximation, which was proposed by Cavata *et al.* [14] and has been widely used [15–19]. The second one is the machine learning method, such as the artificial neural network (ANN) [7–9], convolutional neural network (CNN), light gradient boosting machine (LightGBM) [10,11], and PointNet models [12]. The third one is a model-independent method for reconstructing experimental impact parameter distributions, which was proposed by Das *et al.* [20] and further developed in Refs. [21–23]. In this paper, we refer to it as the Bayesian method.

The first and second methods assume that the observables have a one-to-one correspondence with b, and this idea has inspired a series of efforts to search for a way to accurately determine impact parameters. However, this assumption fails for intermediate energy HICs, because the strong fluctuations of observables with respect to b have been observed in experiments and transport model simulations [16,24–28]. Consequently, different values of the observables can coexist in simulations even for the same impact parameter. Conversely, the same value of the observable could correspond to the different impact parameters. But, these situations also raise a question of whether one can use as many observables as possible to determine b uniquely. Otherwise, one should reconstruct impact parameter distributions from the HIC observables.

The third method considers the fluctuation mechanism of the observables for b and reconstructs the impact parameter distribution from a selected sample of events. This method is based on Bayes's theorem,

$$P(b|X) = P(b)P(X|b)/P(X). \tag{1}$$

$P(X)$ is the probability density of the observable X which can be measured in the experiment, $P(X|b)$ is the probability

*These authors contributed equally to this paper.
†cuiying@ciae.ac.cn
‡zhyx@ciae.ac.cn

density distribution of X at given impact parameter b. The form of $P(X|b)$, also named as the fluctuation kernel [22], is assumed to be a Gaussian [20] or gamma distribution [21] for taking into account the fluctuation. Usually, the observable X was chosen as the multiplicity of charged particles [20–22]. The centroid and width of the Gaussian distribution, or the shape and scale of the gamma distribution are assumed in advance and they depend on b. The values of these parameters were determined by reproducing the experimental data of $P(X)$ with the formula $P(X) = \int P(X|b)P(b)db$. To avoid the uncertainties in the overall impact parameter distributions of $P(b)$, Das *et al.* introduced b centrality [20], i.e., $c_b = \int_0^b P(b')db'$, to replace the variable b. The replacement leads to $P(c_b) = 1$, and $P(X) = \int P(X|c_b)dc_b$. By fitting the data of $P(X)$, one can find the solution of $P(X|c_b)$ and then $P(c_b|X)$ can be obtained based on Bayes's theorem. Then the expected impact parameter distributions of selected events can be retrieved from $P(b|X) = P(b)P(c_b|X)$ [22]. In those works, they mainly focused on how to obtain the impact parameter distribution model-independently with different forms of fluctuation kernel, but discussed less the origin of the fluctuation kernel in physics. Furthermore, one may expect to use the Bayesian method to reconstruct the impact parameter distribution from multiple observables, which may reveal the correlation between different observables as a function of centrality. A related issue has been discussed in Ref. [23] for high energy HICs, but there is no work using this method in low-intermediate energy HICs.

In this work, we investigate whether one can use as many observables as possible to uniquely determine b by exploring the fluctuation mechanism within the framework of the improved quantum molecular dynamics (ImQMD) model [29,30]. Then, we adopt the Bayesian method to reconstruct the impact parameter distributions from two observables, i.e., the multiplicity of charged particles M and total transverse momentum of light particles, $p_t^{\rm tot}$, for selected event samples or centrality. In addition, the uncertainties and bias of the reconstructed covariance matrix elements, which represent the fluctuation of the multiplicity and total transverse momentum of light particles, are discussed. For the selection of event samples in the multidimensional observables space, we propose to use an unsupervised machine learning algorithm, K-means, to automatically handle it.

II. FLUCTUATION MECHANISM IN THE IMQMD MODEL

Now, let us investigate the origins of the fluctuation in HICs and why the impact parameter cannot be uniquely determined with as many observables of the HICs as possible.

Theoretically, the fluctuation of final observables in HICs arises from the many-body correlation term in the transport equation. In the Boltzmann-Uehling-Uhlenbeck model, it can be realized by involving the fluctuation term [24,31–36]. In the quantum molecular dynamics model, it can be realized by involving both the microscopic stochasticity of initialization and nucleon-nucleon collisions with the fixed width of the Gaussian wave packet.

To quantitatively illustrate them in the framework of quantum molecular dynamics model, we perform the calculations of ^{112}Sn + ^{112}Sn at $b = 2$ fm with the ImQMD model [29] under different strengths of initial fluctuations and nucleon-nucleon collisions. The different strengths of the initial fluctuation are realized by using two kinds of initialization, i.e., standard and perturbative initializations. The different strengths of nucleon-nucleon collisions are realized by choosing different bombarding energies, i.e., $E_{\rm beam} = 50$ and 120 MeV/u, and by switching on and off the nucleon-nucleon collisions (named the full and Vlasov modes in this paper).

The standard initialization means that the positions of nucleons are sampled within the radius of nuclei, and the momenta of nucleons are sampled within the Fermi momentum which depends on the local density. The initial nuclei are finally selected under the requirements of fitting the binding energy (for more details see Ref. [30]). In the ImQMD simulations, the HICs are simulated event by event and the initial nuclei of different events are different in microscopic states or in the 6-A dimensional phase space. Quantitatively, we define a dimensionless distance between the first event and kth event in phase space as

$$D_{1k} = \sqrt{\sum_{i=1}^{A}\left[\frac{[\mathbf{x}_1(i)-\mathbf{x}_k(i)]^2}{R_0^2} + \frac{[\mathbf{p}_1(i)-\mathbf{p}_k(i)]^2}{P_0^2}\right]}, \quad (2)$$

to describe the strength of the initial fluctuation between first and kth events. In Eq. (2), the radius of compound nuclei, i.e., $R_0 = 1.2(A_p + A_t)^{1/3}$ fm, and $P_0 = 0.263$ GeV/c are used to normalize the coordinate and momentum to dimensionless variables. A_p and A_t are the numbers of nucleons of the projectile and the target nuclei, respectively. The summation in Eq. (2) runs over all nucleons in the system. For the standard initialization, the distribution of D_{1k} has a Gaussian shape, and its averaged value $\langle D_{1k}\rangle$ and standard deviation (or the width of distribution) $\sigma_{D_{1k}}$ are about 18.0 and 2.0 with the normalization factors R_0 and P_0. The perturbative initialization means that the initialization between any two events has a very tiny difference in phase space. In this work, we set $D_{1k} < 10^{-7}$ at the initial stage between the first and kth events which is far less than the distance for standard initialization. By comparing the results obtained with two kinds of initialization, one can understand the fluctuation originated from initializations.

We then perform the calculations by using two different initializations within the full and Vlasov modes, respectively. Figures 1(a) and 1(c) show the height normalized distribution of the multiplicity of charged particles, i.e., $P(M)/P_{\rm max}(M)$, in the full and Vlasov modes with two kinds of initialization. Two beam energies are simulated: one is 50 MeV/u (red lines) and the other is 120 MeV/u (blue lines). In the full mode, results obtained with both the standard initialization (solid lines) and perturbative initialization (dashed lines) show a Gaussian shape, but the widths of the distributions are different. As listed in Table I, the widths of the distributions obtained with the standard initialization are larger than those with the perturbative initialization. In the case of the Vlasov mode, the multiplicity distributions for two kinds of initialization become completely different. As shown in panel (c), the multiplicity distributions in the case of the standard initialization still keep a Gaussian shape and have widths

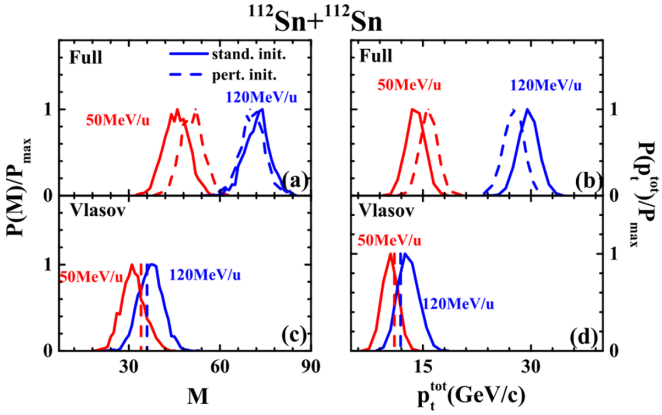

FIG. 1. Height normalized distributions of M and $p_t^{\rm tot}$ obtained with the full mode [panels (a) and (b)] and Vlasov mode [panels (c) and (d)] under the conditions of standard initialization and perturbative initialization. The calculations are performed for ^{112}Sn + ^{112}Sn at $b = 2$ fm.

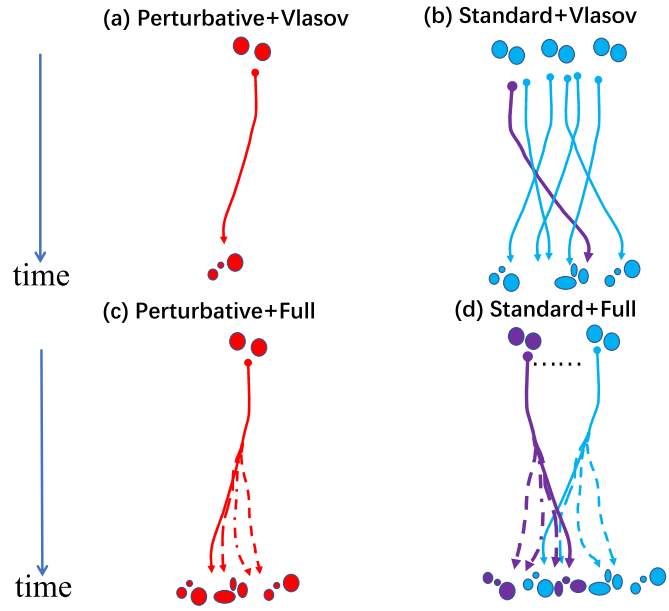

FIG. 2. Sketch of trajectories for different events in the cases of perturbative and standard initialization with Vlasov mode and full mode.

of about ≈20, but the multiplicity distributions in the case of the perturbative initialization become δ distributions due to the absence of the large fluctuation caused by stochastic nucleon-nucleon collisions.

The behaviors mentioned above can be understood from the philosophies of the QMD appoach, which are presented as a sketch in Fig. 2. For convenience, let us start from the Vlasov mode. The lines in Figs. 2(a) and 2(b) represent Vlasov trajectories of events for perturbative and standard initializations in phase space, respectively. In the Vlasov mode, the particles experience only the self-consistent effective mean field, so that the final observables are strongly correlated to the strength of the initial fluctuation. Consequently, the perturbative initialization leads to a δ distribution of final observables, as shown in Fig. 1(c). However, a wide distribution of final observables from different events appears with the standard initialization, as shown in Fig. 1(c), which is attributed to the large strength of fluctuation of the initialization.

For the full mode, there is a wide distribution of final observables from different events even for the perturbative initialization. It comes from the various stochastic nucleon-nucleon collisions, and we depicted it as the dashed lines in Fig. 2(c). In the standard initialization, both the initialization and stochastic nucleon-nucleon collision influence the distribution of final observables, which is illustrated in Fig. 2(d). The widths of distributions of observables increase a little bit compared to the results of the perturbative initialization as shown in Table I because the trajectories of different events are independent in the QMD approach.

TABLE I. The widths of multiplicity distributions from standard and perturbative initializations in the cases of full and Vlasov modes. The numbers in brackets are the widths of distribution of total transverse momentum of light particles.

Mode	$E_{\rm beam}$ (MeV/u)	Stand. init.	Pert. init.
Full	50	4.13 (1.25)	3.74 (1.17)
Full	120	4.13 (1.39)	3.97 (1.35)
Vlasov	50	3.87 (1.17)	0 (0)
Vlasov	120	3.99 (1.37)	0 (0)

The total transverse momentum distribution of light charged particles, i.e., $p_t^{\rm tot} = \sum_i p_t(i)$, obtained by the summation of transverse momentum for light particles with $Z \leqslant 2$, also shows a Gaussian-type distribution, as shown in Figs. 1(b) and 1(d). The results from the full mode and Vlasov mode confirmed again the roles of the initialization and collisions in fluctuation.

Based on the above discussions, one can definitely draw a conclusion that accurate determination of the impact parameter is impossible even with as many HIC observations as possible. The reason is that the one-to-one correspondence between the final observables and the initial states is destroyed by the initial fluctuation and random nucleon-nucleon scattering.

III. PROBABILITY DENSITY FUNCTION $P(\mathbf{X} = \{M_0, p_{t0}^{\rm tot}\}|b)$ FROM PSEUDOEVENT DATA

To get the impact parameter distributions with the Bayesian method from two observables, M and $p_t^{\rm tot}$, one has to first determine the probability density function (PDF) of the observable vector $\mathbf{X} = \{M, p_t^{\rm tot}\}$ at given impact parameter b, i.e., $f(\mathbf{X}, b) = P(\mathbf{X}|b)$, named the fluctuation kernel as in Ref. [22]. In this work, two methods are used to extract the PDF from the pseudodata which is generated by the ImQMD model [29]. One is named direct calculation, which means calculating the distributions of the observables at given b, i.e., $P(\mathbf{X}|b)$, and thus is model dependent. Another is named the reconstructing method, which means fitting the "measured" data of $P(\mathbf{X})$ to reconstruct $P(\mathbf{X}|b)$. The second method only needs the "measured" data of $P(\mathbf{X})$ without knowing the b in advance, and thus is model independent.

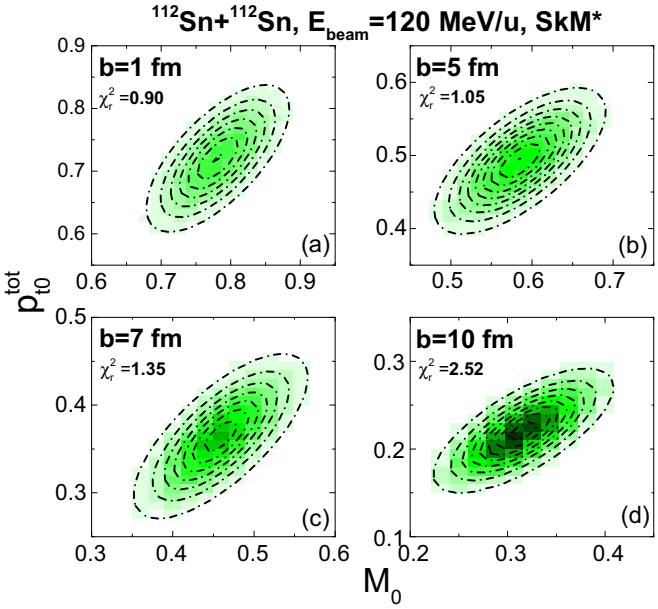

FIG. 3. Contour plots of probability density distribution M_0 vs $p_{t0}^{\rm tot}$. Panel (a) is for 1 fm, (b) is for 5 fm, (c) is for 7 fm, (d) is for 10 fm. The black dashed lines are the results obtained with the assumed PDF formula.

The calculations with the ImQMD model are performed for ^{112}Sn + ^{112}Sn at $E_{\rm beam} = 120$ and 50 MeV/u for generating the pseudodata. The pseudodata contain the information of the real impact parameter and can be used to check the validity of the second method. The number of events is 1 000 000, and the impact parameter b is randomly distributed in the range from 0 to $b_{\rm max} = 1.2(A_p^{1/3} + A_t^{1/3})$ fm according to the probability density $2b/b_{\rm max}^2$.

A. Direct calculation of $P(\mathbf{X}|b)$

As an example, Fig. 3 shows the contour plots of two observables distribution, i.e., P(M_0, $p_{t0}^{\rm tot}$) with $M_0 = M/M_{\rm max}$ and $p_{t0}^{\rm tot} = p_t^{\rm tot}/p_{t,\rm max}^{\rm tot}$, which is obtained with the ImQMD model for ^{112}Sn + ^{112}Sn at 120 MeV/u. The number of events at each b is 60 000. $M_{\rm max}$ and $p_{t,\rm max}^{\rm tot}$ are the maximum multiplicity of charged particles and the maximum total transverse momentum of light charged particles in the calculations, respectively. The values of them in our calculations can be found in Table II. The panels (a), (b), (c), and (d) are the results obtained at $b = 1$, 5, 7, and 10 fm, respectively. The two-dimensional PDFs of $\mathbf{X} = \{M_0, p_{t0}^{\rm tot}\}$ distribute as a Gaussian shape.

TABLE II. Maximum multiplicity of charged particles and total transverse momentum of light charged particles used in system ^{112}Sn + ^{112}Sn for different beam energies.

System	$E_{\rm beam}$ (MeV/u)	$M_{\rm max}$	$p_{t,\rm max}^{\rm tot}$ (GeV/c)
^{112}Sn + ^{112}Sn	50	61	16
	120	86	30

TABLE III. The χ_r^2 of each fitting at different impact parameters for ^{112}Sn + ^{112}Sn and $E_{\rm beam} = 120$ and 50 MeV/u.

	b (fm)	0.0	1.0	2.0	3.0	4.0	5.0
120 MeV/u	χ_r^2	0.96	0.90	1.01	1.01	1.07	1.05
50 MeV/u	χ_r^2	0.96	1.06	1.01	1.12	1.13	1.04
	b (fm)	6.0	7.0	8.0	9.0	10.0	11.0
120 MeV/u	χ_r^2	1.27	1.35	1.50	1.85	2.52	2.89
50 MeV/u	χ_r^2	1.07	1.07	1.16	1.20	1.34	1.34

Except for the ImQMD simulations, the selection of Gaussian form of the PDFs is also a result of probability theory. As we know, the particles are detected with probability p or not with probability $1 - p$ for one event in experiments. It leads to a binomial distribution of observables. If the number of events is large enough, the binomial distribution tends to a Gaussian distribution according to the central limit theorem.

Based on previous discussions, one can assume a two-dimensional Gaussian form of the PDF of M_0 and $p_{t0}^{\rm tot}$ as

$$P(\mathbf{X}|b) = \frac{\exp\left\{-\frac{1}{2}[\mathbf{X} - \overline{\mathbf{X}}(b)]^T \Sigma^{-1}(b)[\mathbf{X} - \overline{\mathbf{X}}(b)]\right\}}{2\pi\sqrt{|\Sigma(b)|}}. \quad (3)$$

$\overline{\mathbf{X}} = \{\overline{M}_0, \overline{p}_{t0}^{\rm tot}\}$ is the mean value of $\mathbf{X}$, and Σ is the symmetric covariance matrix. Σ^{-1} denotes the inverse matrix and $|\Sigma|$ is the determinant. By fitting the ImQMD results at different b with Eq. (3), one can get the form of the PDF (dashed lines in Fig. 3) and the b dependence of $\overline{\mathbf{X}}$, Σ. This is named the direct fitting calculation. The reduced chi-square χ_r^2 values of the fitting at different impact parameters for $E_{\rm beam} = 120$ and 50 MeV/u are listed in Table III, and the values of $\chi_r^2 \leqslant 3$ over the whole range of impact parameters. The form of Gaussisan shape becomes relatively worse at very peripheral collisions due to the limitation of the range of impact parameter.

In Figs. 4(a)–4(f) we present A [$= 1/(2\pi\sqrt{|\Sigma|})$], $\overline{M}_0$, $\overline{p}_{t0}^{\rm tot}$, Σ_{11}, $\Sigma_{12}(\Sigma_{21})$, and Σ_{22} as functions of b for ^{112}Sn + ^{112}Sn at $E_{\rm beam} = 120$ MeV/u. Figure 5 shows similar results at incident energy $E_{\rm beam} = 50$ MeV/u. The open circles are obtained from the direct fitting calculations. $\overline{M}_0$ and $\overline{p}_{t0}^{\rm tot}$ decrease with increasing impact parameter due to the decrease of the size of overlap region and the nucleon-nucleon collision frequency with increasing impact parameter. In addition, Σ_{11}, $\Sigma_{12}(\Sigma_{21})$, and Σ_{22} decrease with increasing impact parameter, which reflects the decrease in the strength of the fluctuation due to the decrease in the nucleon-nucleon collision rate.

The solid circles in panels (a)–(f) are obtained from the mean values, variance, and covariance of observables from their distributions at different b, i.e., by using the following equations:

$$\overline{M}_0(b) = \langle M_0(b)\rangle, \quad (4)$$

$$\overline{p}_{t0}^{\rm tot}(b) = \langle p_{t0}^{\rm tot}(b)\rangle, \quad (5)$$

$$\Sigma_{11}(b) = \langle (M_0 - \overline{M}_0)^2\rangle, \quad (6)$$

$$\Sigma_{22}(b) = \langle (p_{t0}^{\rm tot} - \overline{p}_{t0}^{\rm tot})^2\rangle, \quad (7)$$

$$\Sigma_{12}(b) = \Sigma_{21}(b) = \langle (M_0 - \overline{M}_0)(p_{t0}^{\rm tot} - \overline{p}_{t0}^{\rm tot})\rangle. \quad (8)$$

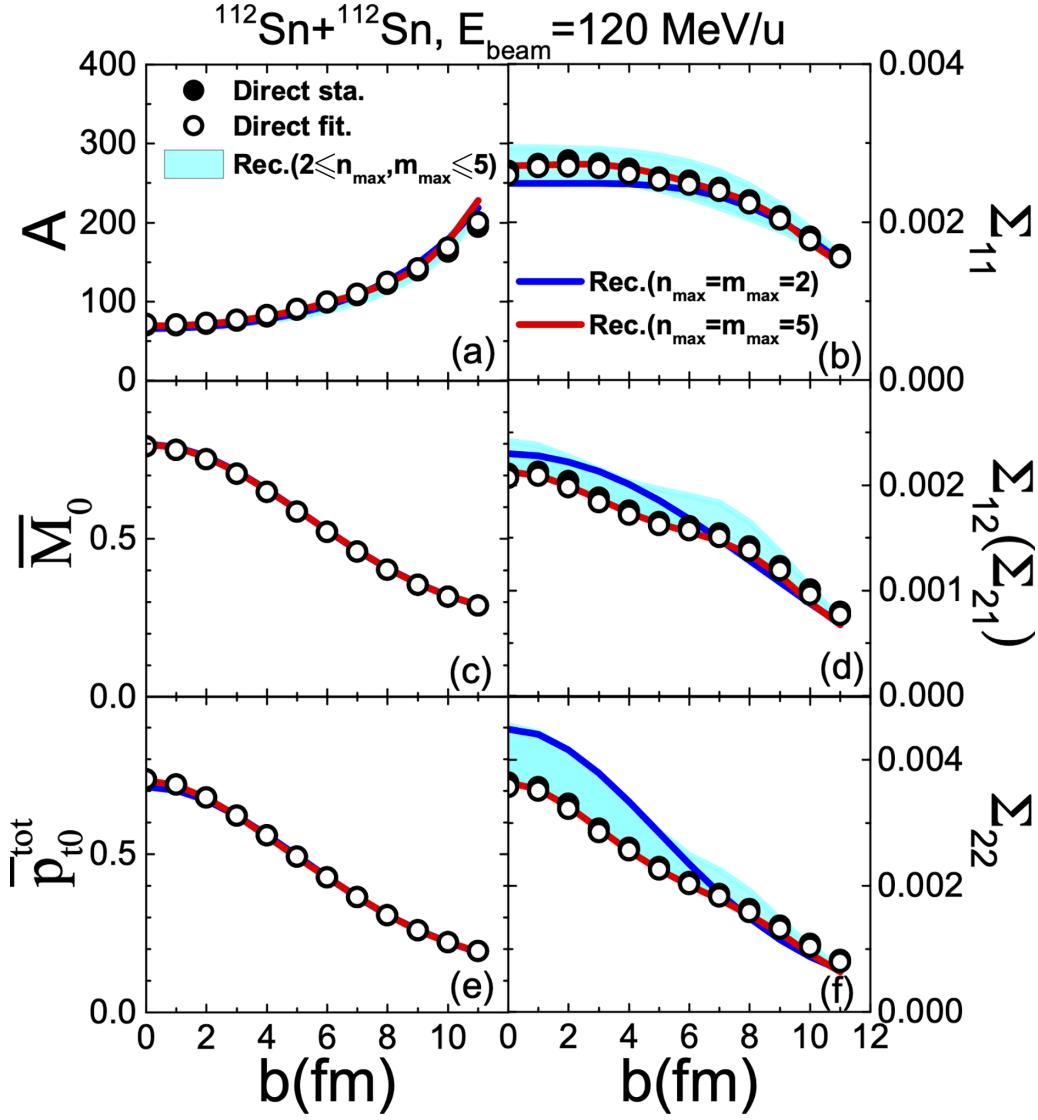

FIG. 4. The parameters A, $\overline{M}_0$, $\overline{p}_{t0}^{\rm tot}$, Σ_{11}, $\Sigma_{12}(\Sigma_{21})$, and Σ_{22} as functions of b for $^{112}\mathrm{Sn}+^{112}\mathrm{Sn}$ at 120 MeV/u. Solid circles are for the direct statistical calculation, the open circles are for the direct fitting calculation, and the cyan shaded regions and the blue and red lines are for the reconstructing method.

$\langle\cdot\rangle$ means an average over the events with the same impact parameter b. We named this method direct statistical calculations. The values obtained from Eqs. (4)–(8) can validate the applicability of the Gaussian PDF and direct fitting method. It is shown in Figs. 4 and 5 that the open circles are very close to the solid circles. The cyan shaded regions are obtained from the reconstructing method by directly fitting the data of $P(\mathbf{X})$, and we will discuss it in Sec. III B.

B. Reconstructing $P(\mathbf{X}|b)$

To reconstruct the impact parameter distribution model-independently, we adopt the formula

$$P(\mathbf{X}) = \int_0^1 P(\mathbf{X}|c_b)P(c_b)dc_b = \int_0^1 P(\mathbf{X}|c_b)dc_b \qquad (9)$$

to fit the data of $P(\mathbf{X})$. In our calculations, the form of $P(\mathbf{X}|c_b)$ is assumed to be

$$P(\mathbf{X}|c_b) = \frac{\exp\left\{-\frac{1}{2}[\mathbf{X}-\overline{\mathbf{X}}(c_b)]^T\Sigma^{-1}(c_b)[\mathbf{X}-\overline{\mathbf{X}}(c_b)]\right\}}{2\pi\sqrt{|\Sigma(c_b)|}}. \qquad (10)$$

The mean values $\overline{\mathbf{X}}$ and the elements of the covariance matrix Σ_{ij} are smooth positive functions of c_b, and are expressed as the exponential of a polynomial as in Ref. [23],

$$\overline{X}_i(c_b) = \overline{X}_i(0)\exp\left(-\sum_{n=1}^{n_{\max}} a_{i,n}c_b^n\right), \qquad (11)$$

$$\Sigma_{ij}(c_b) = \Sigma_{ij}(0)\exp\left(-\sum_{m=1}^{m_{\max}} A_{ij,m}c_b^m\right). \qquad (12)$$

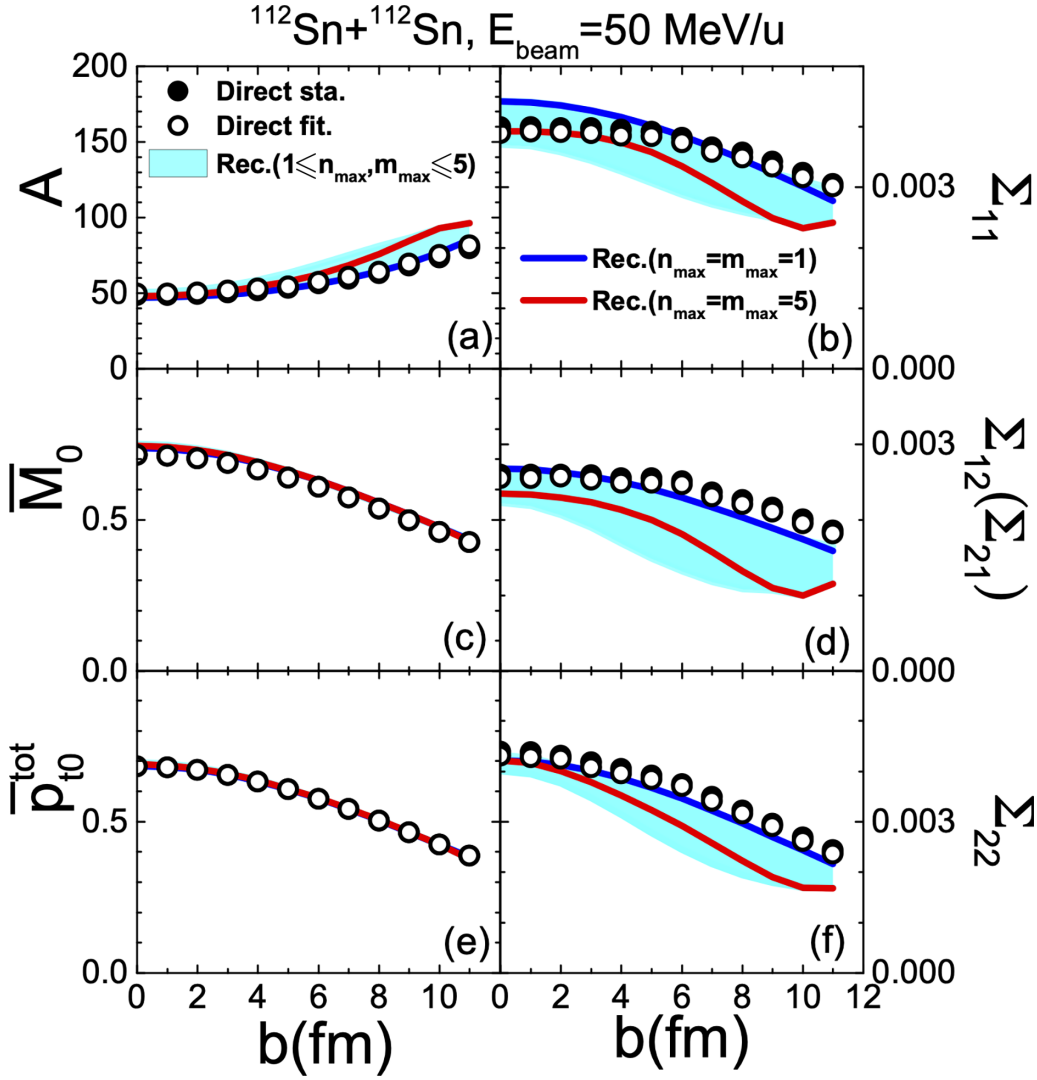

FIG. 5. Same as Fig. 4, but for $E_{\rm beam} = 50$ MeV/u.

where $\overline{X}_i(0)$, $a_{i,n}$, $\Sigma_{ij}(0)$, $A_{ij,m}$ are free parameters, and $n_{\rm max}$ and $m_{\rm max}$ are the degrees of the polynomials used to parametrize the mean and the covariance. These parameters are adjusted to obtain the best fit of $P(\mathbf{X})$ by using the code MINUIT.

To directly view the validity of the reconstructing method, we first present the contour plot of $P(\mathbf{X})$ obtained with the ImQMD model (color map) and reconstructing method (red solid lines), which corresponds to the minimum fitting parameters when $\chi_r^2 < 2$ in Figs. 6(a) and 7(a). The panels (b) and (c) in Figs. 6 and 7 are contour plots of $P(\mathbf{X}|b)$, obtained by direct fitting calculations (black dashed lines), and by the reconstructing method at $b = 1$ fm and $b = 7$ fm, respectively. The reconstructing method can well reproduce both the data and the results from the direct fitting calculation when $b \geqslant 7$ fm at 120 MeV/u. For central collisions, the reconstructed $P(\mathbf{X}|b)$ slightly deviates from the data along the $p_{t0}^{\rm tot}$ direction. At incident energy of $E_{\rm beam} = 50$ MeV/u, as shown in Figs. 7(b) and 7(c), the reconstructing method can reproduce the shape of $P(\mathbf{X}|b)$ but the mean M_0 value of the Gaussian form deviates from the real value less than 5%.

The key point in the reconstruction is to find a reasonable number of the degrees of the polynomials, i.e., $n_{\rm max}$ and $m_{\rm max}$. When $n_{\rm max}$ and $m_{\rm max}$ are too small, the Bayesian method may not reproduce $P(\mathbf{X})$. Conversely, when the $n_{\rm max}$ and $m_{\rm max}$ are too large, one may confront an overfitting issue. In experiments, it is hard to justify how many fitting parameters are good enough by only seeking the minimum of χ_r^2 among the different parameter sets, since the real b dependence of $\overline{X}_i$ and Σ_{ij} or the real b distribution are not known in advance. Consequently, we need to learn the uncertainties of the reconstructed results by using different combinations of $n_{\rm max}$ and $m_{\rm max}$, and the deviation (or bias) relative to the true values.

For ^{112}Sn + ^{112}Sn at $E_{\rm beam} = 120$ MeV/u, $n_{\rm max} = m_{\rm max} = 1$ cannot reproduce $P(\mathbf{X})$ and the corresponding χ_r^2 is about 23. When $2 \leqslant n_{\rm max} \leqslant 5$ and $2 \leqslant m_{\rm max} \leqslant 5$, the obtained χ_r^2 values are in the range 1.26–1.64. $n_{\rm max} > 5$ and $m_{\rm max} > 5$ were not used due to the number of fitting parameters exceeding the limit of the MINUIT. In Fig. 4, $\overline{X}_i(b)$ and $\Sigma_{ij}(b)$ obtained with $2 \leqslant n_{\rm max} \leqslant 5$ and $2 \leqslant m_{\rm max} \leqslant 5$ are presented as cyan-shaded regions, which reflect the uncertainties caused by different choices of $n_{\rm max}$ and $m_{\rm max}$. The uncertainties of

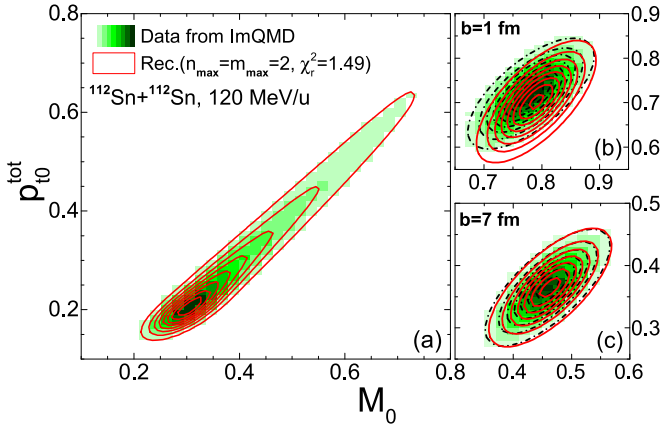

FIG. 6. Contour plots of probability density distribution M_0 vs $p_{t0}^{\rm tot}$ for $^{112}{\rm Sn}+^{112}{\rm Sn}$ at $E_{\rm beam}=120$ MeV/u. The red solid lines are the results obtained from the reconstructing method; the black dashed lines are from the direct fitting calculation.

$\overline{X}_i$ are less than 1.4%, and the uncertainties of Σ_{ij} are less than 14%.

In Figs. 8(a)–8(c), the deviations of Σ_{ij} at 120 MeV/u are presented by using the ratios between the reconstructed fitting parameters and direct fitting parameters. The blue lines are the results obtained with $n_{\rm max}=m_{\rm max}=2$, which is selected based on the maxim that fewer parameters are preferred than more if all of them can fit the data. In this case, the deviations of Σ_{11} is less than 10%, and the large deviations appear at $b<5$ fm for Σ_{12} and Σ_{22} and its values reach 33%. The red lines are the results obtained with $n_{\rm max}=m_{\rm max}=5$, and the reconstructing method ($n_{\rm max}=m_{\rm max}=5$) can reproduce the results of direct calculation. The slight deviations appears at very peripheral collisions.

For $^{112}{\rm Sn}+^{112}{\rm Sn}$ at $E_{\rm beam}=50$ MeV/u, the reconstructed Σ_{ij} are presented in Fig. 5. The cyan-shaded region corresponds to the uncertainties obtained with $1\leqslant n_{\rm max}\leqslant 5$ and $1\leqslant m_{\rm max}\leqslant 5$, where the values of χ_r^2 are in the range 1.03–1.42. The uncertainties of $\overline{X}_i$ are less than 1%, and the uncertainties of Σ_{ij} are less than 31%. In Fig. 8(d)–8(f) the deviations of Σ_{ij} are presented. When $n_{\rm max}\geqslant 2$ and $m_{\rm max}\geqslant 2$, the reconstructed Σ_{ij} are lower than that from those of the direct calculations. The reconstructed Σ_{ij} with $n_{\rm max}=m_{\rm max}=1$

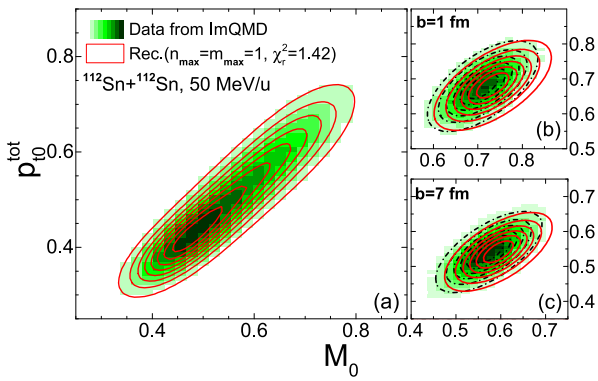

FIG. 7. Same as Fig. 6, but for $E_{\rm beam}=50$ MeV/u.

(blue lines) are close to that obtained with the direct calculations within 14%, and the deviations appear at both central and peripheral collisions. The red lines are the results obtained with $n_{\rm max}=m_{\rm max}=5$. At $b<3$ fm, the deviations are less than 12%. With the impact parameter increasing, the deviations increase and the largest deviation occur around $b=9.5$ fm.

One should note that the multiplicities and total transverse momenta obtained in the ImQMD model are overestimated compared with the experimental data, which are related to the stability of initial nuclei [2,37,38] and cluster formation mechanism [39–43] in the QMD type models. It may influence the absolute values of reconstructed $\overline{X}_i$ and Σ_{ij}, but it will not obviously influence the shape of $P(\mathbf{X})$ and the reconstruction.

IV. BAYESIAN METHOD FOR RECONSTRUCTING IMPACT PARAMETER DISTRIBUTION FROM TWO OBSERVABLES

A. Sorting centrality with *K*-means

Before reconstructing the impact parameter distribution from two observables for selected events or the centrality with Bayes's theorem, we need to find a way to sort the events with $\mathbf{X}=\{M_0, p_{t0}^{\rm tot}\}$ and define the centrality of HICs. Differently from using a single observable, the simultaneous use of M_0 and $p_{t0}^{\rm tot}$ will make difficulties in the determination of the upper and lower boundaries of $\mathbf{X}$. One may artificially define the region in the space of $\mathbf{X}$, for example, a rectangle shape, an elliptic shape, or other shapes, to select the events. This ambiguous criterion requires us to find a rule to sort the centrality of HICs in two-observable space, i.e., M_0 and $p_{t0}^{\rm tot}$ space. Compared to the traditional method, the unsupervised machine learning clustering algorithms [44,45], i.e., the *K*-means clustering method, can automatically classify the events into different classes once the number of classes is given.

The *K*-means clustering method is one of the simplest and commonly used unsupervised machine learning algorithms. It tries to find cluster centers that are representative of certain regions of the data without knowing the label of data points. In this work, the dataset $D=\{\mathbf{X}_i=(M_0, p_{t0}^{\rm tot})_i\}$ with $i=1,\ldots,N_{\rm event}$ and $N_{\rm event}=1\,000\,000$ is generated from the ImQMD model. We classify the dataset into K clusters, i.e., $C=\{C_1, C_2, \ldots, C_K\}$. C_i represents the subdataset of the ith classification, which is realized by the alternation between two steps: assigning each data point to the closest cluster center where the distance is defined by $d_{ij}=\sqrt{(X_i-X_j)^2}$, and then setting each cluster center as the mean of the data points that are assigned to it. When the assignment of instances to clusters, i.e.,

$$E=\sum_{k=1}^{K}\sum_{X_i\in C_k}|X_i-\mu_k|^2, \tag{13}$$

where μ_k is the center of cluster k, no longer changes, the algorithm will be finished.

There is a question raised for us: why we can use the unsupervised *K*-means clustering method to sort the centrality of HICs? It can be answered from Eq. (13). Suppose the total

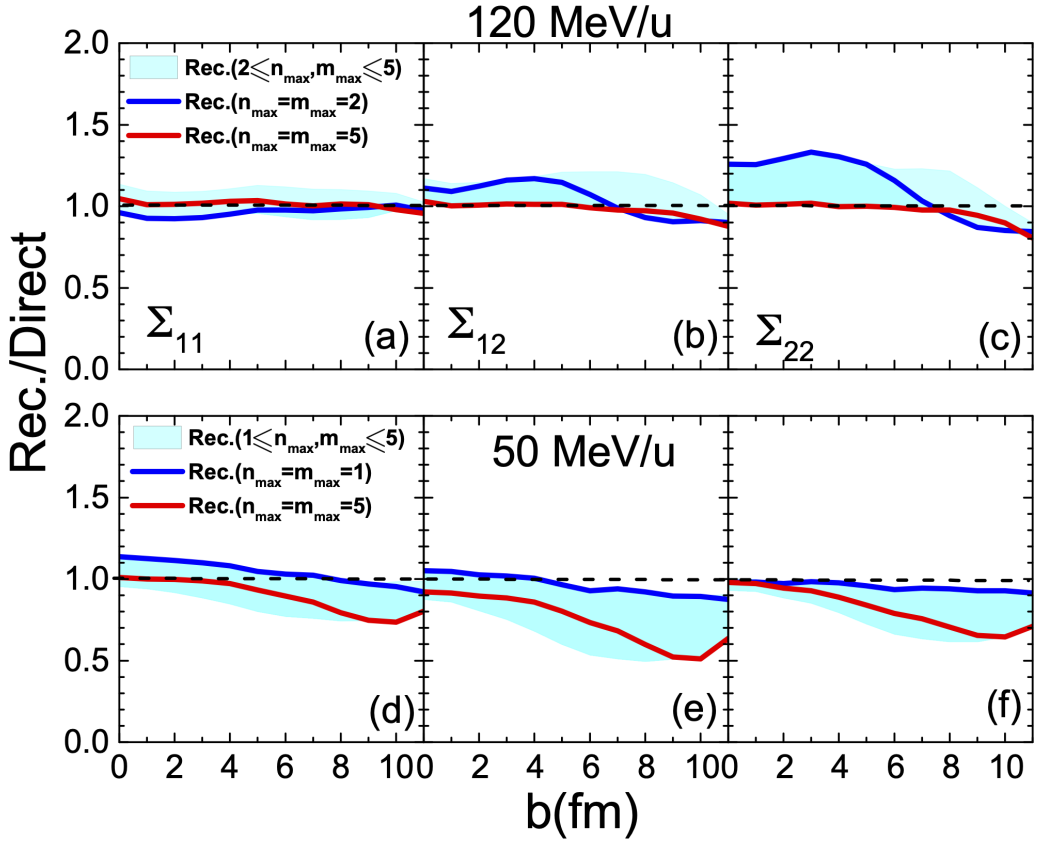

FIG. 8. The ratio of the reconstructing method and direct fitting calculation about Σ_{11}, Σ_{12}, and Σ_{22} as functions of b for $^{112}\mathrm{Sn} + ^{112}\mathrm{Sn}$ at 120 (upper panels) and 50 (lower panels) MeV/u.

number of event points in the dataset is N_0 and the number of event points in C_k is N_k. Based on the previous notification and properties of clusters, the centroid of each cluster is written as

$$\mu_k = \frac{1}{N_k}\sum_{\mathbf{i}\in C_k}\mathbf{X}_i. \tag{14}$$

As we prove in the Appendix, the centroid of cluster is related to the centrality of selected events as follows:

$$\begin{aligned}\mu_k &\approx \frac{N_0\mathbf{X}^*}{N_k}\sum_{\mathbf{X}\in\Omega(C_k)} P(\mathbf{X})\cdot\Delta s \\ &= \frac{N_0\mathbf{X}^*}{N_k}c(C_k).\end{aligned} \tag{15}$$

Here, $\Delta s = dM_0 dp_{t0}^{\mathrm{tot}}$ and $c(C_k)$ is the centrality defined from the event points of cluster C_k, i.e.,

$$c(C_k) = \sum_{\mathbf{X}\in\Omega(C_k)} P(\mathbf{X})\cdot\Delta s, \tag{16}$$

which is similar to the idea of experimental centrality by Abelev *et al.* [20,22,23,46]. $\mathbf{X}^*$ is a certain value that satisfies the equality of

$$\sum_{\mathbf{X}\in\Omega(C_k)} P_{\in C_k}(\mathbf{X})\cdot\mathbf{X}\cdot\Delta s = \mathbf{X}^*\sum_{\mathbf{X}\in\Omega(C_k)} P(\mathbf{X})\cdot\Delta s. \tag{17}$$

Thus, the K-means clustering algorithm can be used to sort the centrality.

B. Reconstruction of impact parameter distribution

Figures 9(a) and 9(c) show the distributions of event points on the M_0 and p_{t0}^{tot} plane for $E_{\mathrm{beam}} = 120$ and 50 MeV/u, respectively. The events points are sorted into five clusters by the K-means clustering algorithm, and are represented by different color regions. The centroids of each cluster are represented by the black solid circles. The overlap between different clusters is less than 10%, and caused by the algorithm for seeking the minimum of Eq. (13). In Figs. 9(b) and 9(d), we plot the predicted reduced impact parameter $b_0 = b/b_{\max}$ distributions by using the Bayesian method, i.e.,

$$P(b|\mathbf{X}\in C_k) = \frac{P(b)\int_{\mathbf{X}\in\Omega(C_k)} P(\mathbf{X}|b)d\mathbf{X}}{\int_{\mathbf{X}\in\Omega(C_k)} P(\mathbf{X})d\mathbf{X}}. \tag{18}$$

Two kinds of $P(\mathbf{X}|b)$ are used. One is direct fitting calculation (dashed lines), and another is the reconstructing method (shaded regions) with different $n_{\max}$ and $m_{\max}$ combinations. The real reduced impact parameter distributions obtained with the ImQMD model (open circles) are used for checking the ability of the two methods. As illustrated in Figs. 9(b) and 9(d), the predicted reduced impact parameter distributions from the reconstructing method agree well with the actual

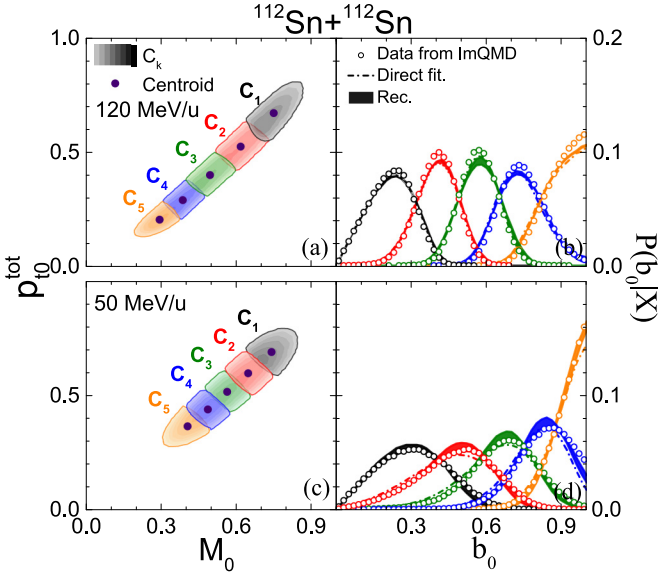

FIG. 9. (a) and (c) Contour plot of M_0 vs $p_{t0}^{\rm tot}$ for five clusters. (b) and (d) Reduced impact parameter distributions for five clusters; open circles are the real impact parameter distributions obtained with ImQMD model, and shaded regions are the results inferred with the reconstructing method with different $n_{\rm max}$ and $m_{\rm max}$ combinations (dashed lines for direct fitting calculation).

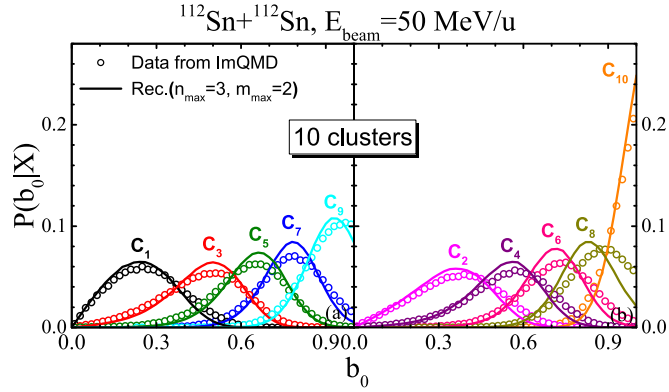

FIG. 10. Same as Fig. 9(d), but for ten clusters. The lines with different colors are the results inferred by the reconstructing method with $n_{\rm max} = 3$ and $m_{\rm max} = 2$.

impact parameter distributions under the different combinations of $n_{\rm max}$ and $m_{\rm max}$, which have $\chi_r^2 < 2$.

The reasons why the reconstructing method can reproduce the real impact parameter distribution and is less influenced by the deviations of the covariance matrix can be understood from the following two aspects: one is the validity of Gaussian assumptions on the $P(\mathbf{X}|b)$, and another is the reconstructing method on $P(b|\mathbf{X})$ based on Eq. (18).

The validity of Gaussian assumptions comes from the reaction mechanism, as discussed in Sec. II. The event-by-event fluctuations of final observables with respect to b are dominated by the mechanism of initialization, the mean field potential, and nucleon-nucleon elastic collisions. In the ImQMD simulations, the sampled events are distributed as a Gaussian form in the event space since the initial nuclei in each event are randomly sampled at a given binding energy and radius of the nucleus. The mean field and nucleon-nucleon elastic collisions do not destroy the Gaussian shape of the fluctuations of observables to b at the beam energy we studied. It is a reason why the χ_r^2 is less than 3 in our studies, as shown in Table III, and are smaller than the χ_r^2 obtained in high energy collisions [23].

The weak influence of Σ_{ij} on the reconstruction of $P(b|\mathbf{X})$, as shown in Fig. 9, is related to the range of $\Omega(C_k)$ in the domain of $\mathbf{X}$. The extreme case is to take only 1 cluster by using K-means; one can expect that the influence of different values of Σ_{ij} completely disappears due to the integration over the full $\mathbf{X}$ space. Quantitatively, in Fig. 10, we present the reconstructed b distributions of $^{112}\mathrm{Sn} + ^{112}\mathrm{Sn}$ at 50 MeV/u for ten clusters. The values $n_{\rm max} = 3$ and $m_{\rm max} = 2$, which correspond to the largest deviations of Σ_{ij} between the reconstructing method and direct fitting calculations, are used to see the effects. The real b distributions for ten clusters are presented as symbols. The left panel is the results from C_1, C_3, ... to C_9 and the right panel is from C_2, C_4, ... to C_{10}. It is clear that the differences between the reconstructed b distribution and real b distribution become larger in the case of ten clusters than that in five clusters [Fig. 9(d)].

V. SUMMARY AND DISCUSSIONS

In summary, we investigate the inherent fluctuation mechanism of intermediate energy heavy ion collisions within the framework of the ImQMD model before studying the reconstruction of the impact parameter distribution from HIC observables. Our calculations show that the inherent fluctuations come from the stochasticity of initialization and nucleon-nucleon scattering in HICs. These inherent fluctuations cause the heavy ion collision observables to fluctuate with b, and an accurate determination of the impact parameter is impossible even with as many observables as possible. Thus, the reconstruction of the impact parameter distribution from the selected HIC observables should be done.

To model-independently reconstruct the impact parameter distributions for the selected centrality or events for low-intermediate energy HICs, we extend the Bayesian method in which two observables, i.e., multiplicity of charged particles and total transverse momentum of light charged particles, are used simultaneously. A two-dimensional Gaussian-shape fluctuation kernel is adopted, and the parameters of the fluctuation kernel are learned model independently by fitting the pseudoevents data. Since the b dependence of mean values and covariance matrix of experimental data are not known in advance, we also investigate the uncertainties of the extracted b dependence of mean values and covariance matrix. With this form of fluctuation kernel of two observables at a given impact parameter b, the impact parameter distributions for selected events can be derived based on Bayes's theorem. For sorting the centrality of heavy ion collisions with multiple observables, we propose to use an unsupervised machine learning method, i.e., the K-means clustering method, which can automatically select the event sample in the multiobservables space if the class number is given. The validity of

using the K-means clustering method to sort the centrality of HICs is also proved in the theory. Our calculations show that the reconstructed b distributions agree well with the real b distributions when the number of sorted centrality is around 5 in this energy region.

Further, the knowledge of the covariance matrix can be used to extract the fluctuations and correlation between the multiplicity of charged particles and the total momentum of light charged particles, which will be useful for learning the fragmentation mechanism.

ACKNOWLEDGMENTS

The authors thank the anonymous referee's helpful comments and suggestions. This work was supported by the National Natural Science Foundation of China under Grants No. 12275359, No. 11875323, No. 11705163, No. 11790320, No. 11790323, and No. 11961141003, by the National Key R&D Program of China under Grant No. 2018 YFA0404404, by the Continuous Basic Scientific Research Project (No. WDJC-2019-13, No. BJ20002501), by funding of the China Institute of Atomic Energy under Grant No. YZ222407001301, and by the Leading Innovation Project of the CNNC under Grants No. LC192209000701 and No. LC202309000201.

APPENDIX: RELATION BETWEEN THE CENTROID OF EACH CLUSTER AND CENTRALITY

The centroid of each cluster,

$$\mu_k = \frac{1}{N_k}\sum_{\mathbf{i}\in C_k}\mathbf{X}_i, \tag{A1}$$

can be rewritten as

$$\begin{aligned}\mu_k &= \frac{1}{N_k}\sum_{\mathbf{X}\in\Omega(C_k)}\frac{N_{C_k}(\mathbf{X})}{\Delta s}\cdot\mathbf{X}\cdot\Delta s \\ &= \frac{N_0}{N_k}\sum_{\mathbf{X}\in\Omega(C_k)}P_{\in C_k}(\mathbf{X})\cdot\mathbf{X}\cdot\Delta s.\end{aligned} \tag{A2}$$

Here, $N_{C_k}(\mathbf{X})$ is the number of events in cluster C_k in the interval $\Delta s = dM_0 dp_{t0}^{\rm tot}$. The values of $\mathbf{X}$ in the C_k cluster appear in the domain of Ω, and their probability density function is $P_{\in C_k}(\mathbf{X})$. In the K-means clustering algorithm, the overlapped event points between different clusters are less than 10%, and thus $P_{C_k}(\mathbf{X}) \approx P(\mathbf{X})$. Consequently, the centroid of each cluster μ_k can be approximately described as follows:

$$\begin{aligned}\mu_k &\approx \frac{N_0\mathbf{X}^*}{N_k}\sum_{\mathbf{X}\in\Omega(C_k)}P(\mathbf{X})\cdot\Delta s \\ &= \frac{N_0\mathbf{X}^*}{N_k}c(C_k).\end{aligned} \tag{A3}$$

$c(C_k)$ is the centrality defined from the event points of cluster C_k, i.e.,

$$c(C_k) = \sum_{\mathbf{X}\in\Omega(C_k)}P(\mathbf{X})\cdot\Delta s, \tag{A4}$$

The definition is similar to the idea of experimental centrality by Abelev *et al.* [46]. $\mathbf{X}^*$ is a certain value that satisfies the equality of

$$\sum_{\mathbf{X}\in\Omega(C_k)}P_{\in C_k}(\mathbf{X})\cdot\mathbf{X}\cdot\Delta s = \mathbf{X}^*\sum_{\mathbf{X}\in\Omega(C_k)}P(\mathbf{X})\cdot\Delta s. \tag{A5}$$

[1] E. E. Kolomeitsev, C. Hartnack, H. W. Barz, M. Bleicher, E. Bratkovskaya, W. Cassing, L. W. Chen, P. Danielewicz, C. Fuchs, T. Gaitanos *et al.*, J. Phys. G: Nucl. Part. Phys. **31**, S741 (2005).

[2] J. Xu, L.-W. Chen, M. B. Tsang, H. Wolter, Y.-X. Zhang, J. Aichelin, M. Colonna, D. Cozma, P. Danielewicz, Z.-Q. Feng, A. LeFevre, T. Gaitanos, C. Hartnack, K. Kim, Y. Kim, C. M. Ko, B. A. Li, Q. F. Li, Z. X. Li, P. Napolitani, A. Ono, M. Papa, T. Song, J. Su, J. L. Tian, N. Wang, Y. J. Wang, J. Weil, W. J. Xie, F. S. Zhang, and G. Q. Zhang, Phys. Rev. C **93**, 044609 (2016).

[3] H. Wolter, M. Colonna, D. Cozma, P. Danielewicz, C. M. Ko, R. Kumar, A. Ono, M. B. Tsang, J. Xu, Y.-X. Zhang *et al.*, Prog. Part. Nucl. Phys. **125**, 103962 (2022).

[4] M. Colonna, Y.-X. Zhang, Y.-J. Wang, D. Cozma, P. Danielewicz, C. M. Ko, A. Ono, M. B. Tsang, R. Wang, H. Wolter *et al.*, Phys. Rev. C **104**, 024603 (2021).

[5] Y.-X. Zhang, Y.-J. Wang, M. Colonna, P. Danielewicz, A. Ono, M. B. Tsang, H. Wolter, J. Xu, L.-W. Chen, D. Cozma *et al.*, Phys. Rev. C **97**, 034625 (2018).

[6] A. Ono, J. Xu, M. Colonna, P. Danielewicz, C. M. Ko, M. B. Tsang, Y.-J. Wang, H. Wolter, Y.-X. Zhang, L.-W. Chen *et al.*, Phys. Rev. C **100**, 044617 (2019).

[7] S. A. Bass, A. Bischoff, C. Hartnack, J. A. Maruhn, J. Reinhardt, H. Stocker, and W. Greiner, J. Phys. G: Nucl. Part. Phys. **20**, L21 (1994).

[8] C. David, M. Freslier, and J. Aichelin, Phys. Rev. C **51**, 1453 (1995).

[9] F. Haddad, K. Hagel, J. Li, N. Mdeiwayeh, J. B. Natowitz, R. Wada, B. Xiao, C. David, M. Freslier, and J. Aichelin, Phys. Rev. C **55**, 1371 (1997).

[10] F. Li, Y. Wang, H. Lü, P. Li, Q. Li, and F. Liu, J. Phys. G: Nucl. Part. Phys. **47**, 115104 (2020).

[11] C. Y. Tsang, Y. Wang, M. B. Tsang, J. Estee, T. Isobe, M. Kaneko, M. Kurata-Nishimura, J. W. Lee, F. Li, Q. Li *et al.*, arXiv:2107.13985.

[12] M. Omana Kuttan, J. Steinheimer, K. Zhou, A. Redelbach, and H. Stoecker, Phys. Lett. B **811**, 135872 (2020).

[13] L. Li, Y. Zhang, Y. Cui, and J. Liang, Sci. Sin. Phys. Mech. Astron. **52**, 252014 (2022).

[14] C. Cavata, M. Demoulins, J. Gosset, M.-C. Lemaire, D. L'Hôte, J. Poitou, and O. Valette, Phys. Rev. C **42**, 1760 (1990).

[15] J. Péter, J. Sullivan, D. Cussol, G. Bizard, R. Brou, M. Louvel, J. Patry, R. Regimbart, J. Steckmeyer, B. Tamain *et al.*, Nucl. Phys. A **519**, 127 (1990).

[16] L. Phair, D. Bowman, C. Gelbke, W. Gong, Y. Kim, M. Lisa, W. Lynch, G. Peaslee, R. de Souza, M. Tsang *et al.*, Nucl. Phys. A **548**, 489 (1992).

[17] J. Łukasik, J. Benlliure, V. Métivier, E. Plagnol, B. Tamain, M. Assenard, G. Auger, C. O. Bacri, E. Bisquer, B. Borderie *et al.*, Phys. Rev. C **55**, 1906 (1997).

[18] A. Andronic, J. Łukasik, W. Reisdorf, and W. Trautmann, Eur. Phys. J. A **30**, 31 (2006).
[19] T. X. Liu, W. G. Lynch, R. H. Showalter, M. B. Tsang, X. D. Liu, W. P. Tan, M. J. van Goethem, G. Verde, A. Wagner, H. F. Xi *et al.*, Phys. Rev. C **86**, 024605 (2012).
[20] S. J. Das, G. Giacalone, P.-A. Monard, and J.-Y. Ollitrault, Phys. Rev. C **97**, 014905 (2018).
[21] R. Rogly, G. Giacalone, and J.-Y. Ollitrault, Phys. Rev. C **98**, 024902 (2018).
[22] J. D. Frankland, D. Gruyer, E. Bonnet, B. Borderie, R. Bougault, A. Chbihi, J. E. Ducret, D. Durand, Q. Fable, M. Henri *et al.* (INDRA Collaboration), Phys. Rev. C **104**, 034609 (2021).
[23] K. Vahid Yousefnia, A. Kotibhaskar, R. Bhalerao, and J.-Y. Ollitrault, Phys. Rev. C **105**, 014907 (2022).
[24] P. Chomaz, M. Colonna, and J. Randrup, Phys. Rep. **389**, 263 (2004).
[25] P.-B. Gossiaux and J. Aichelin, Phys. Rev. C **56**, 2109 (1997).
[26] C. A. Ogilvie, D. A. Cebra, J. Clayton, S. Howden, J. Karn, A. Vander Molen, G. D. Westfall, W. K. Wilson, and J. S. Winfield, Phys. Rev. C **40**, 654 (1989).
[27] Y. Zhang, X. Wu, and Z. Li, Phys. Rev. C **69**, 044609 (2004).
[28] L. Li, Y. Zhang, Z. Li, N. Wang, Y. Cui, and J. Winkelbauer, Phys. Rev. C **97**, 044606 (2018).
[29] Y. Zhang, M. Tsang, Z. Li, and H. Liu, Phys. Lett. B **732**, 186 (2014).
[30] Y.-X. Zhang, N. Wang, Q.-F. Li, L. Ou, J.-L. Tian, M. Liu, K. Zhao, X.-Z. Wu, and Z.-X. Li, Front. Phys. **15**, 54301 (2020).
[31] F.-S. Zhang and E. Suraud, Phys. Lett. B **319**, 35 (1993).
[32] M. Colonna, M. Di Toro, A. Guarnera, S. Maccarone, M. Zielinska-Pfabé, and H. Wolter, Nucl. Phys. A **642**, 449 (1998).
[33] M. Colonna, Phys. Rev. Lett. **110**, 042701 (2013).
[34] W.-J. Xie, J. Su, L. Zhu, and F.-S. Zhang, Phys. Lett. B **718**, 1510 (2013).
[35] P. Napolitani and M. Colonna, Phys. Lett. B **726**, 382 (2013).
[36] P. Napolitani and M. Colonna, Phys. Rev. C **92**, 034607 (2015).
[37] J. Yang, Y. Zhang, N. Wang, and Z. Li, Phys. Rev. C **104**, 024605 (2021).
[38] J. Aichelin, Phys. Rep. **202**, 233 (1991).
[39] R. Nebauer, J. Aichelin, INDRA Collaboration, M. Assenard, G. Auger, Ch. O. Bacri, F. Bocage, R. Bougault, R. Brou, P. Buchet, J. L. Charvet *et al.*, Nucl. Phys. A **658**, 67 (1999).
[40] Y. Zhang and Z. Li, Phys. Rev. C **71**, 024604 (2005).
[41] K. Zbiri, A. Le Fèvre, J. Aichelin, J. Łukasik, W. Reisdorf, F. Gulminelli, U. Lynen, W. F. J. Müller, H. Orth, C. Schwarz, C. Sfienti, W. Trautmann, K. Turzo, B. Zwieglinski, J. L. Charvet, A. Chbihi, R. Dayras, D. Durand, J. D. Frankland, R. Legrain, N. LeNeindre, O. Lopez, L. Nalpas, M. Parlog, E. Plagnol, M. F. Rivet, E. Rosato, E. Vient, M. Vigilante, C. Volant, and J. P. Wieleczko (ALADIN Collaboration and INDRA Collaboration), Phys. Rev. C **75**, 034612 (2007).
[42] P. Danielewicz and G. Bertsch, Nucl. Phys. A **533**, 712 (1991).
[43] Ono, Akira, EPJ Web Conf. **117**, 07003 (2016).
[44] J. B. Macqueen, *Proceedings of the Fifth Berkeley Symposium on Mathematical Statistics and Probability* (University of California Press, Oakland, 1967).
[45] S. V. D. Arthur, *Proceedings of the Eighteenth Annual ACM-SIAM Symposium on Discrete Algorithms* (Society for Industrial and Applied Mathematics, Philadelphia, 2007).
[46] B. Abelev, J. Adam, D. Adamová, A. M. Adare, M. M. Aggarwal, G. Aglieri Rinella, M. Agnello, A. G. Agocs, A. Agostinelli, Z. Ahammed *et al.* (ALICE Collaboration), Phys. Rev. C **88**, 044909 (2013).